Journal of Alloys and Compounds 509S (2011) S629–S632

Contents lists available at ScienceDirect

Journal of Alloys and Compounds

journal homepage: www.elsevier.com/locate/jallcom

Hydrogen desorption properties of melt-spun and hydrogenated Mg-based alloys using in situ synchrotron X-ray diffraction and TGA

Siarhei Kalinichenka[a], Lars Röntzsch[b,*], Carsten Baehtz[c], Thomas Weißgärber[b], Bernd Kieback[a,b]

[a] Institute for Materials Science, Dresden University of Technology, Helmholtzstraße 7, 01069 Dresden, Germany
[b] Fraunhofer Institute for Manufacturing Technology and Applied Materials Research IFAM, Winterbergstraße 28, 01277 Dresden, Germany
[c] Institute of Ion Beam Physics and Materials Research, Forschungszentrum Dresden-Rossendorf, Bautzner Landstraße 400, 01328 Dresden, Germany

ARTICLE INFO

Article history:
Received 23 July 2010
Received in revised form
28 September 2010
Accepted 11 October 2010
Available online 23 October 2010

Keywords:
Hydrogen storage material
Metal hydride
Magnesium alloy
Mg
Ni
Cu
Y
Melt spinning
Nanocrystallinity
Dehydrogenation kinetics
In situ synchrotron X-ray diffraction
TGA

ABSTRACT

Three magnesium-based alloys, $Mg_{90}Ni_{10}$, $Mg_{80}Ni_{10}Y_{10}$ and $Mg_{85}Cu_5Ni_5Y_5$, were prepared by melt-spinning and compared regarding their hydrogen desorption properties. Their hydrogen desorption kinetics after activation and hydrogenation was investigated by thermogravimetry at different temperatures in the range from 150 °C to 250 °C. It was found that $Mg_{80}Ni_{10}Y_{10}$ exhibits a much faster desorption kinetics in comparison to $Mg_{90}Ni_{10}$ and $Mg_{85}Cu_5Ni_5Y_5$ of up to 1.3 wt.%-H_2/min. The corresponding crystal phase transformations were investigated in detail by in situ synchrotron X-ray diffraction. It was found that the kinetics of hydrogenation is controlled by different reaction pathways for $Mg_{90}Ni_{10}$, $Mg_{80}Ni_{10}Y_{10}$ and $Mg_{85}Cu_5Ni_5Y_5$.

1. Introduction

Magnesium alloys are widely known and have been investigated in view of their application as reversible hydrogen storage materials [1]. They are particularly attractive candidates for the solid-state hydrogen storage because of the high gravimetric hydrogen storage density of up to 7.6 wt.%-H_2 in the case of MgH_2, low specific weight, a comparatively high abundance in the earth's crust and low cost of magnesium as base metal [2]. Nevertheless, the slow hydrogen sorption kinetics and the high reactivity with water and oxygen are still challenges in view of practical application.

In order to enhance the hydrogenation and dehydrogenation kinetics, magnesium alloys should have a sub-micrometer crystal size and should contain catalytically active elements like transition metals, metal oxides, or rare earth elements in order to enhance the dehydrogenation and hydrogenation kinetics [3]. For this purpose, Mg alloys can be ground by high-energy ball-milling techniques to reduce the average grain size and to disperse such catalyst particles [4,5]. Alternatively, nanocrystalline Mg alloys can be produced by rapid solidification processes like melt-spinning [6–10]. With this high-yield rapid cooling technique an amorphous or super-fine microstructure solidifies in the form of ribbons which are several tens of micrometer thin.

Melt-spun Mg alloys exhibit good hydrogen storage properties based on the reaction of hydrogen gas with the solid material [9]. However, structural phase transformation during the hydrogen sorption reactions and the role of catalyst particles still need to be investigated in detail to elucidate the complex reaction pathways. In the present contribution, we focus on the phase transformations during desorption of thee melt-spun, activated and hydrogenated magnesium-rich Mg–Ni, Mg–Ni–Y and Mg–Cu–Ni–Y alloys ($Mg_{90}Ni_{10}$, $Mg_{80}Ni_{10}Y_{10}$ and $Mg_{85}Cu_5Ni_5Y_5$) whose hydrogen storage characteristics were studied recently [9,10,11]. In order to understand the dehydrogenation reactions of the melt-spun and activated alloys, the desorption properties have been studied by in situ synchrotron X-ray diffraction (SR-XRD) as well as by thermogravimetric analysis using a magnetic suspension balance. It is well known, that in situ synchrotron X-ray powder diffraction can pro-

* Corresponding author. Tel.: +49 351 253 7411; fax: +49 351 253 7399.
E-mail address: Lars.Roentzsch@ifam-dd.fraunhofer.de (L. Röntzsch).

0925-8388/$ – see front matter © 2010 Elsevier B.V. All rights reserved.
doi:10.1016/j.jallcom.2010.10.067

vide important information during the processes of crystallization and, furthermore, kinetic data for the absorption/desorption processes [12,13]. The experiments were performed at the Rossendorf Beamline (BM20) of the European Synchrotron Radiation Facility (ESRF) in Grenoble.

2. Experimental

2.1. Materials and preparation methods

Mg–Ni–Y and Mg–Cu–Ni–Y master alloys ingots with the chemical compositions $Mg_{80}Ni_{10}Y_{10}$ and $Mg_{85}Cu_5Ni_5Y_5$ were produced by induction-melting of a mixture of pure Mg (99.9% purity) metal, Ni (99.9% purity) powder, Cu (99.99% purity) powder and a Ni–Y alloy (Ni–25.4 wt.%; Y–75.5 wt.%) in a tantalum crucible at 1000 °C under argon atmosphere. For production of the $Mg_{90}Ni_{10}$ master alloy, appropriate amounts of the raw materials (Mg and Ni) were mixed together and melted in an induction furnace using a BN coated crucible under argon. During melt-spinning of these alloys, continuous ribbons with 35 μm in thickness and 10 mm in width were obtained from a single roller melt-spinning device (PSI) which contains a copper wheel with a diameter of 200 mm and a constant surface velocity of 40 m/s as rapid cooling component. The melt-spinning experiments were carried our under argon atmosphere.

The thermal activation of the melt-spun ribbons was achieved during three cycles at 385 °C and pressures between 2 and 30 bar H_2 (99.9998% purity) for 11 h.

2.2. Analysis

The dehydrogenation kinetics was examined by thermogravimetry (TGA) using a magnetic suspension balance (Rubotherm) in vacuum (10^{-2} mbar H_2). Additionally, in situ SR-XRD studies were performed at the Rossendorf Beamline (ROBL-CRG, BM20) of the European Synchrotron Radiation Facility (ESRF) in Grenoble. In the case of $Mg_{90}Ni_{10}$ and $Mg_{80}Ni_{10}Y_{10}$ the measurements were carried out in a special annealing chamber, using a hemispherical radiation window (Be-dome), which allows in-plane and out-of-plane measurements in horizontal and vertical directions. For $Mg_{85}Cu_5Ni_5Y_5$, a stainless steel annealing chamber with kapton windows was used for in situ SR-XRD. For preparation, the hydrogenated ribbons were manually ground into fine powders by adding acetone. A small amount of the sample was put together with a thermocouple onto a Si single crystal sample holder. The incident X-ray beam with an X-ray wavelength of 1.05 Å was used for investigating the scanning range of the diffraction angle between 13.5° and 28° (2Θ) in reflection geometry. The angular step was 0.02° and the fixed count mode at a rate of 10,000 counts per step was applied for the measurements. The temperature of the sample under study was automatically controlled and measured using a thermocouple directly placed in contact with the sample. The evolution of the peaks of the crystalline phases was then recorded in situ, using an high-load scintillation detector.

Microstructural characterization of hydrogenated $Mg_{85}Cu_5Ni_5Y_5$ has been carried out using a transmission electron microscope (TEM). High-angle annular dark field imaging in STEM mode was performed using a FEI Tecnai F30. For TEM sample preparation, the hydrogenated alloys were manually ground into a fine powder, dispersed in ethanol and drop-deposited on a Ni micro-grid.

3. Results and discussion

3.1. Structural characterization of hydrogenated ribbons

The crystalline phases of all the investigated alloys after activation and 11.5 hydrogenation–dehydrogenation cycles were identified using SR-XRD analysis as presented in Fig. 1. Hydrogenated $Mg_{90}Ni_{10}$ consists of four hydride phases (MgH_2, high temperature (HT) and low temperature (LT) Mg_2NiH_4 and $Mg_2NiH_{0.3}$) as well as of crystalline hcp Mg. The presence of metallic Mg indicates the incomplete hydrogenation of the sample. The pattern of hydrogenated $Mg_{80}Ni_{10}Y_{10}$ exhibits five different hydride phases: MgH_2, HT- and LT-Mg_2NiH_4, YH_2 and YH_3. The pattern of hydrogenated $Mg_{85}Cu_5Ni_5Y_5$ reveals also five hydride phases: MgH_2, high temperature Mg_2NiH_4, $Mg_2NiH_{0.3}$, YH_2, YH_3 as well as $MgCu_2$. The presence of $MgCu_2$ in the alloy suggests the reaction of Mg_2Cu with hydrogen according to Eq. (1):

$$2Mg_2Cu + 3H_2 \rightleftarrows 3MgH_2 + MgCu_2 \quad (1)$$

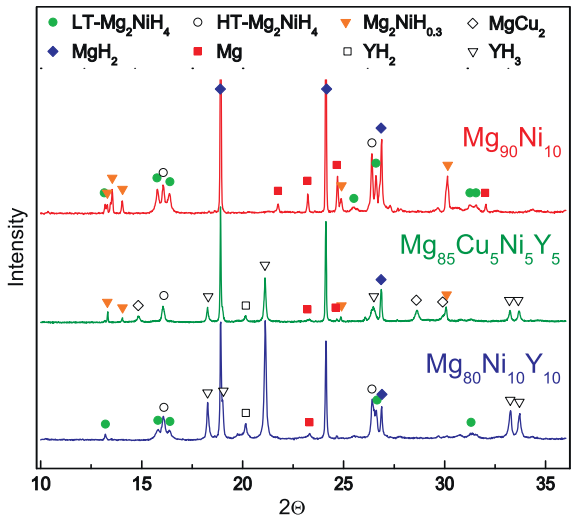

Fig. 1. Synchrotron X-ray diffraction patterns of melt-spun and hydrogenated $Mg_{90}Ni_{10}$, $Mg_{80}Ni_{10}Y_{10}$ and $Mg_{85}Cu_5Ni_5Y_5$.

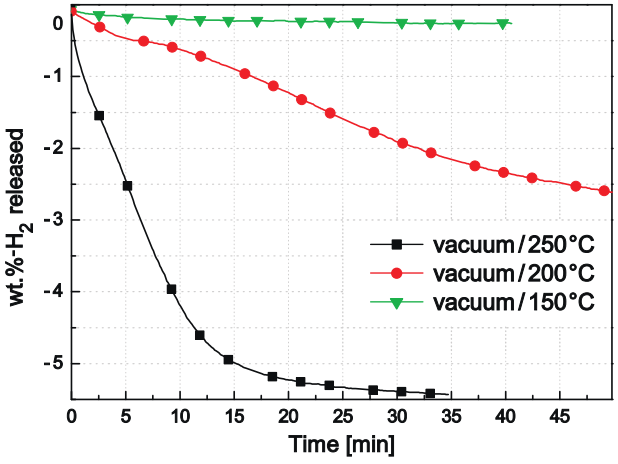

Fig. 2. Hydrogen desorption kinetics of $Mg_{85}Cu_5Ni_5Y_5$ at different temperatures and at a pressure of 10^{-2} mbar H_2.

3.2. Desorption characteristics of hydrogenated alloys using TGA and in situ synchrotron X-ray diffraction

After sample activation, the desorption characteristics of the hydrogenated alloys were studied by thermogravimetry using a magnetic suspension balance. The results for $Mg_{90}Ni_{10}$ and $Mg_{80}Ni_{10}Y_{10}$ were presented in our previous paper [10]. Fig. 2 depicts hydrogen desorption kinetics of $Mg_{85}Cu_5Ni_5Y_5$ at different temperatures at a pressure of 10^{-2} mbar H_2.

The dehydrogenation rates of all alloys were calculated from TGA data and summarized in Table 1. It is evident that the hydrogen desorption kinetics strongly depends on the desorption temperature. The largest dehydrogenation rate at all measured condition exhibits $Mg_{80}Ni_{10}Y_{10}$ at 250 °C (1.3 wt.%-H_2/min).

Table 1
Dehydrogenation rates of $Mg_{90}Ni_{10}$, $Mg_{80}Ni_{10}Y_{10}$ and $Mg_{85}Cu_5Ni_5Y_5$ at different temperatures.

Hydrogen pressure	10^{-2} mbar			
Temperature [°C]	250	200	180	150
Dehydrogenation rate [wt.%-H_2/min]				
$Mg_{90}Ni_{10}$ [10]	0.7	0.07	~0	~0
$Mg_{80}Ni_{10}Y_{10}$ [10]	1.3	0.18	0.07	~0
$Mg_{85}Cu_5Ni_5Y_5$	0.5	0.065	–	~0

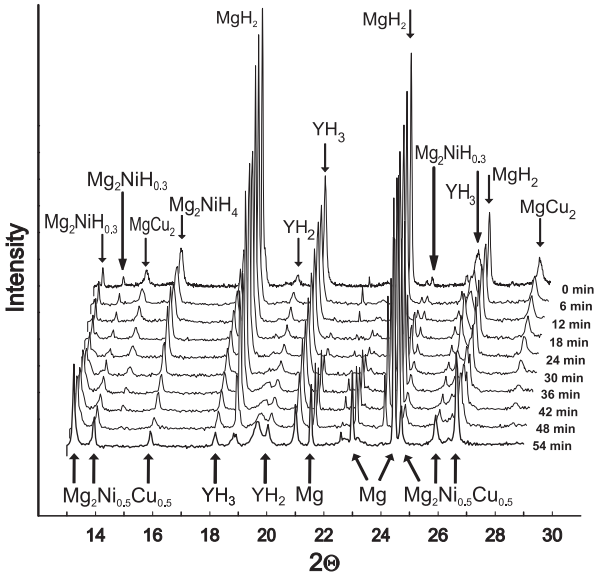

Fig. 3. The evolution of the in situ synchrotron XRD pattern of melt-spun and hydrogenated $Mg_{85}Cu_5Ni_5Y_5$ during its isothermal dehydrogenation at 200 °C and at a pressure of 10^{-2} mbar H_2.

In order to understand the interplay of different catalyst phases during the thermal decomposition, the hydrogen desorption reactions were studied by in situ synchrotron X-ray diffraction (SR-XRD).

According to the results obtained by SR-XRD for $Mg_{90}Ni_{10}$ and $Mg_{80}Ni_{10}Y_{10}$ these alloys undergo a complex sequence of dehydrogenation reactions [10]. In the case of $Mg_{90}Ni_{10}$ the vacuum thermal desorption can be divided into three steps:

- Step 1: Dehydrogenation of Mg_2NiH_4 to $Mg_2NiH_{0.3}$.
- Step 2: Dehydrogenation of MgH_2 in the presence of $Mg_2NiH_{0.3}$ to Mg.
- Step 3: Dehydrogenation of $Mg_2NiH_{0.3}$ to Mg_2Ni.

The SR-XRD results of decomposition of hydrogenated $Mg_{80}Ni_{10}Y_{10}$ showed that the dehydrogenation of MgH_2 and Mg_2NiH_4 at 200 °C was almost completed within 24 min. These results are in accordance with those obtained by TGA measurement [10]. It must be also noticed that no formation of $Mg_2NiH_{0.3}$ was observed in the case of $Mg_{80}Ni_{10}Y_{10}$ during dehydrogenation. The reason for this behaviour may be explained by the fact that yttrium can be solved in Mg_2Ni causing a lattice parameter expansion which could lead to a fast and direct dehydrogenation of Mg_2NiH_4 into Mg_2Ni [10].

The evolution of the in situ SR-XRD patterns of the as-spun and hydrogenated $Mg_{85}Cu_5Ni_5Y_5$ during vacuum thermal decomposition at 200 °C (10^{-2} mbar) is presented in Fig. 3. The X-ray diffraction pattern at $t = 0$ min corresponds to the hydrogenated state at ambient temperature. The heating to 200 °C was carried out within the first 4 min.

During the dehydrogenation of $Mg_{85}Cu_5Ni_5Y_5$ several processes can be identified: decomposition of the hydride phases according to Eqs. (2)–(5) and transformation of $MgCu_2$ and formation of $Mg_2Ni_{0.5}Cu_{0.5}$.

$$MgH_2 \rightarrow Mg + H_2 \quad (2)$$

$$Mg_2NiH_4 \rightarrow Mg_2NiH_{0.3} + 1.85H_2 \quad (3)$$

$$Mg_2NiH_{0.3} \rightarrow Mg_2Ni + 0.15H_2 \quad (4)$$

$$2YH_3 \rightarrow 2YH_2 + H_2 \quad (5)$$

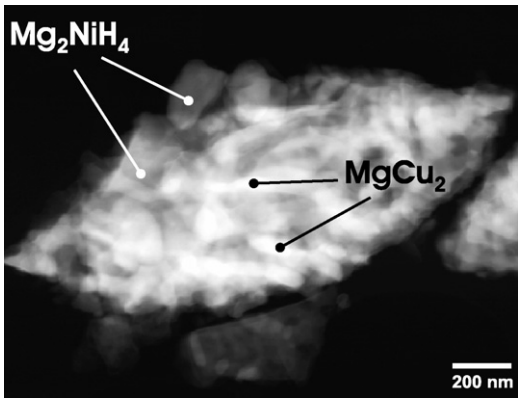

Fig. 4. High angle annular dark field scanning TEM image of a domain which contains Mg_2NiH_4 and $MgCu_2$ and which is embedded in the MgH_2 matrix.

However, it seems in contrast to $Mg_{90}Ni_{10}$ and $Mg_{80}Ni_{10}Y_{10}$ that these dehydrogenation reactions take place simultaneously. After dehydrogenation four phases have been observed in the material: Mg, $Mg_2Ni_{0.5}Cu_{0.5}$, YH_2 and YH_3. These XRD results of the dehydrogenated sample are similar to literature data, e.g. for $Mg_{60}Ni_{10}Cu_{30}$ prepared by ball milling [14].

It is well known that Cu and Mg_2Ni form Cu-substituted Mg_2Ni ($Mg_2Ni_{1-x}Cu_x$). This alloys exhibit a large homogeneity range for x values up to 0.85 [15]. In our investigation we observed the formation of the hexagonal $Mg_2Ni_{0.5}Cu_{0.5}$ phase. The cell parameters obtained from the X-ray patterns for this alloy ($a = 5.22$ Å and $b = 13.51$ Å) are in good agreement with literature data [15,16]. From the XRD results, the hydrogen release reaction between Mg_2NiH_4, MgH_2 and $MgCu_2$ may be described with the following equation [14]:

$$0.75MgH_2 + 0.25MgCu_2 + 0.5Mg_2NiH_4 \rightarrow Mg_2Ni_{0.5}Cu_{0.5} + 1.75H_2 \quad (6)$$

It is also evident that the transformation of YH_3 into YH_2 is the slowest step of the reaction and even after 54 min at 200 °C a residual amount of YH_3 can be observed in the diffraction pattern.

The peak at ~19.5 2Θ cannot be identified unambiguously; it probably corresponds to Mg- or Y-oxide.

TEM investigations of hydrogenated $Mg_{85}Cu_5Ni_5Y_5$ revealed that domains, in which the phases Mg_2NiH_4 and $MgCu_2$ are agglomerated (cf. Fig. 4), are embedded in the MgH_2 matrix in addition to finely dispersed yttrium hydride particles [10]. These domains have dimensions of 1–3 μm. However, the individual Mg_2NiH_4 and $MgCu_2$ grains therein have been found in the dimension of 100 nm (cf. Fig. 4). This finding demonstrates that the catalytically active phases Mg–Cu and Mg–Ni are not finely dispersed in MgH_2 matrix. This phenomenon may be due to a co-formation of Mg_2Ni and Mg_2Cu (or $Mg_2Ni_{0.5}Cu_{0.5}$) during crystallization of the melt-spun alloys and subsequent hydrogenation into Mg_2NiH_4 and $MgCu_2$. The model describing the catalytic effect of Mg_2Cu suggested by Karty et al. [17] states that Mg_2Cu dissociates hydrogen easily which is then delivered to the adjacent Mg phase forming MgH_2 (hydrogen transfer phase). In the present case of hydrogenated $Mg_{85}Cu_5Ni_5Y_5$ no direct Mg/Mg_2Cu interface could be observed. Hence, the hydrogen transfer from Mg_2Cu to Mg/MgH_2 is hindered. This is consistent with the TGA measurement (cf. Fig. 2) in which the overall kinetics for hydrogen desorption is rather slow compared to $Mg_{90}Ni_{10}$ and $Mg_{80}Ni_{10}Y_{10}$ (cf. Table 1). Nevertheless, in order to better understand the role of the different catalyst phases during hydrogen desorption of hydrogenated $Mg_{85}Cu_5Ni_5Y_5$ further in situ investigations are being performed [11].

4. Conclusion

In this contribution, we have compared hydrogen desorption kinetics of three magnesium-base alloys, $Mg_{90}Ni_{10}$, $Mg_{80}Ni_{10}Y_{10}$ and $Mg_{85}Cu_5Ni_5Y_5$ prepared by melt-spinning. Dehydrogenation rates of all alloys at different temperatures in the range from 150 °C to 250 °C were presented. Using in situ synchrotron X-ray diffraction it was found that the alloys show different reactions during the dehydrogenation. Hence, the kinetics of dehydrogenation is controlled by different mechanisms. In the case of $Mg_{90}Ni_{10}$ two separate processes were identified: desorption of Mg_2NiH_4 to $Mg_2NiH_{0.3}$ and desorption of MgH_2 in the presence of $Mg_2NiH_{0.3}$. Thus, it is evident that $Mg_2NiH_{0.3}$ acts as a hydrogen transfer phase for the dehydrogenation of MgH_2 [10]. In situ SR-XRD investigations of the thermal decomposition of $Mg_{80}Ni_{10}Y_{10}$ showed no formation of $Mg_2NiH_{0.3}$ during dehydrogenation. The reason for this finding could be explained by yttrium which is dissolved in Mg_2Ni [18]. Compared to $Mg_{90}Ni_{10}$ and $Mg_{80}Ni_{10}Y_{10}$, it was found that $Mg_{85}Cu_5Ni_5Y_5$ exhibits slower dehydrogenation rates, even though the content of catalytic elements is higher in $Mg_{85}Cu_5Ni_5Y_5$ than in $Mg_{90}Ni_{10}$. The SR-XRD results indicate that the dehydrogenation of the hydride phases, the transformation of $MgCu_2$ and formation of $Mg_2Ni_{0.5}Cu_{0.5}$ take place at the same time. It must be also mentioned that no formation of Mg_2Cu was observed during the dehydrogenation of $Mg_{85}Cu_5Ni_5Y_5$. In melt-spun and hydrogenated $Mg_{85}Cu_5Ni_5Y_5$, the $MgCu_2$ phase exists in direct contact with Mg_2NiH_4 and is not finely dispersed in the Mg/MgH_2 matrix as TEM analysis reveals. Thus, the specific interface area between Mg and $MgCu_2$ is rather small which leads to the conclusion that the additional catalytic effect of $MgCu_2$ on the hydrogen sorption properties of rapidly solidified Mg–Ni–Y alloys is negligible. However, more detailed studies of the microstructure evolution and the hydrogen sorption behaviour of melt-spun Mg–Cu–Ni–Y alloys are required and will be published elsewhere [11].

Acknowledgements

The authors would like to acknowledge financial support from the Boysen-Stiftung, the Fraunhofer Attract program and the European Synchrotron Radiation Facility. Further, we thank Th. Riedl for TEM analyses as well as M. Hesse and Th. Schmidt for their practical support.

References

[1] B. Sakintuna, F. Lamari-Darkrim, M. Hirscher, Int. J. Hydrogen Energy 32 (9) (2007) 1121–1140.
[2] I.P. Jain, C. Lal, A. Jain, Int. J. Hydrogen Energy 35 (10) (2010) 5133–5144.
[3] M. Fichtner, Adv. Eng. Mater. 7 (2005) 443–455.
[4] G. Liang, J. Huot, S. Boily, A. Van Neste, R. Schulz, J. Alloys Compd. 292 (1–2) (1999) 247–252.
[5] O. Gutfleisch, S. Dal Toè, M. Herrich, A. Handstein, A. Pratt, J. Alloys Compd. 404–406 (2005) 413–416.
[6] T. Spassov, U. Köster, J. Alloys Compd. 287 (1–2) (1999) 243–250.
[7] T. Spassov, U. Lyubenova, U. Köster, M.D. Barò, Mater. Sci. Eng. A 375–377 (2004) 794–799.
[8] M.Y. Song, S. Kwon, J.S. Bae, S.-H. Hong, Int. J. Hydrogen Energy 33 (6) (2008) 1711–1718.
[9] S. Kalinichenka, L. Röntzsch, B. Kieback, Int. J. Hydrogen Energy 34 (18) (2009) 7749–7755.
[10] S. Kalinichenka, L. Röntzsch, C. Baehtz, B. Kieback, J. Alloys Compd. 496 (1–2) (2010) 608–613.
[11] S. Kalinichenka, L. Röntzsch, Th. Riedl, Th. Gemming, B. Kieback, Int. J. Hydrogen Energy, accepted for publication.
[12] R.V. Denys, A.B. Riabov, J.P. Maehlen, M.V. Lototsky, J.K. Solberg, V.A. Yartys, Acta Mater. 57 (2009) 3989–4000.
[13] A. Teresiak, A. Gebert, M. Savyak, M. Uhlemann, Ch. Mickel, N. Mattern, J. Alloys Compd. 398 (2005) 156–164.
[14] C. Milanese, A. Girella, G. Bruni, P. Cofrancesco, V. Berbenni, P. Matteazzi, A. Marini, Intermetallics 18 (2) (2010) 203–211.
[15] P. Darnaudery, M. Pezat, B. Darriet, J. Less-Common Met. 92 (1983) 199–205.
[16] P. Selvam, B. Viswanathan, C.S. Swamy, V. Srinivasan, Int. J. Hydrogen Energy 13 (1988) 87–94.
[17] A. Karty, J. Genossar, P.S. Rudman, J. Appl. Phys. 50 (11) (1979) 7200–7209.
[18] N. Cui, B. Luan, H.J. Zhao, H.K. Liu, S.X. Dou, J. Alloys Compd. 233 (1–2) (1996) 236–240.